KIF13B enhances the endocytosis of LRP1 by recruiting LRP1 to caveolae

Yoshimitsu Kanai,[1] Daliang Wang,[1] and Nobutaka Hirokawa[1,2]

[1]Department of Cell Biology and Anatomy, Graduate School of Medicine, The University of Tokyo, Tokyo 113-0033, Japan
[2]Center of Excellence in Genomic Medicine Research, King Abdulaziz University, Jeddah, 21589, Saudi Arabia

Multifunctional low-density lipoprotein (LDL) receptor-related protein 1 (LRP1) recognizes and internalizes a large number of diverse ligands, including LDL and factor VIII. However, little is known about the regulation of LRP1 endocytosis. Here, we show that a microtubule-based motor protein, KIF13B, in an unexpected and unconventional function, enhances caveolin-dependent endocytosis of LRP1. KIF13B was highly expressed in the liver and was localized on the sinusoidal plasma membrane of hepatocytes. KIF13B knockout (KO) mice showed elevated levels of serum cholesterol and factor VIII, and KO MEFs showed decreased uptake of LDL. Exogenous KIF13B, initially localized on the plasma membrane with caveolae, was translocated to the vesicles in the cytoplasm with LRP1 and caveolin-1. KIF13B bound to hDLG1 and utrophin, which, in turn, bound to LRP1 and caveolae, respectively. These linkages were required for the KIF13B-enhanced endocytosis of LRP1. Thus, we propose that KIF13B, working as a scaffold, recruits LRP1 to caveolae via LRP1–hDLG1–KIF13B–utrophin–caveolae linkage and enhances the endocytosis of LRP1.

Introduction

Kinesin superfamily proteins (KIFs) play essential roles in the intracellular transport of various cargos, such as membranous organelles, protein complexes, and mRNA within cells (Hirokawa, 1998; Vale, 2003; Hirokawa et al., 2010). KIF13B is a kinesin-3 family motor protein that binds to centaurin-α1 and hDLG1 via its forkhead-associated (FHA) and membrane-associated guanylate kinase homologue binding stalk (MBS) domains, respectively (Hanada et al., 2000; Miki et al., 2001; Venkateswarlu et al., 2005). KIF13B activates Arf6 function by inhibiting the Arf6-GAP activity of centaurin-α1 (Venkateswarlu et al., 2005), and several reports have indicated it may bind to cargo via centaurin-α1 or hDLG1 (Horiguchi et al., 2006; Bolis et al., 2009). However, the cargo of KIF13B has not yet been identified, and little is known about the role of KIF13B in animal models. In this study, we elucidate a new scaffolding role of KIF13B in caveolin-dependent endocytosis of low-density lipoprotein (LDL) receptor–related protein 1 (LRP1).

LRP1 is the most multifunctional member of the LDL receptor family, and it is expressed in a wide variety of tissues (Herz and Strickland, 2001). It is suggested to have two main biological functions: endocytosis of its numerous ligands and regulation of cell signaling pathways. LRP1 interacts with and mediates the endocytosis of more than 40 ligands, including lipoproteins, proteinases, proteinase–inhibitor complexes, extracellular matrix proteins, bacterial toxins, viruses, and various intracellular proteins (Herz et al., 1992; Kounnas et al., 1995; Liu et al., 2000; Wang et al., 2003). LRP1 is endocytosed by clathrin- and caveolin-dependent pathways (Zhang et al., 2004). However, little is known about how LRP1 is linked to the endocytic pathways, and how the endocytosis of LRP1 is regulated.

Here, we show that KIF13B enhances caveolin-dependent endocytosis of LRP1 by recruiting LRP1 to caveolae. KIF13B was highly expressed in the liver and was localized on the sinusoidal plasma membrane of hepatocytes. Disruption of the KIF13B gene caused increased levels of serum cholesterol and factor VIII (fVIII) in animals and decreased uptake of LDL in KIF13B-deficient cells. Exogenous KIF13B, initially localized on the plasma membrane with caveolae, was translocated to the vesicles in the cytoplasm with LRP1 and caveolin-1. We identified utrophin as a new KIF13B binding protein. KIF13B bound

Correspondence to Nobutaka Hirokawa: hirokawa@m.u-tokyo.ac.jp

Abbreviations used in this paper: βDG, β-dystroglycan; FHA, forkhead associated; fVIII, factor VIII; HDL, high-density lipoprotein; KIF, kinesin superfamily protein; KO, knockout; LDL, low-density lipoprotein; LDLr, LDL receptor; LRP1, LDL receptor–related protein 1; MBS, membrane-associated guanylate kinase homologue binding stalk; MEF, mouse embryonic fibroblast; WT, wild type.

The Rockefeller University Press $30.00
J. Cell Biol. Vol. 204 No. 3 395–408
www.jcb.org/cgi/doi/10.1083/jcb.201309066

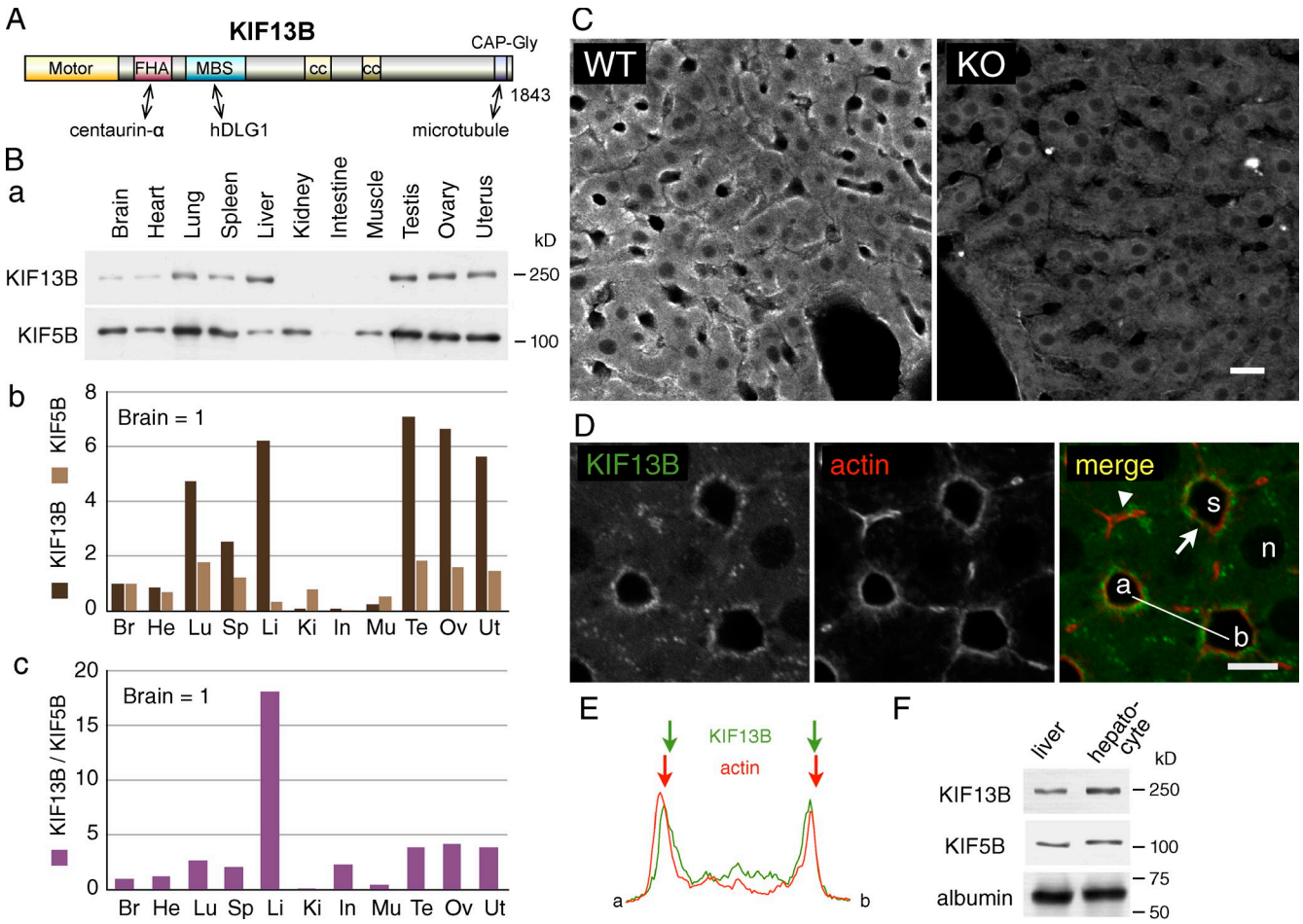

Figure 1. **KIF13B is localized on the sinusoidal plasma membrane of hepatocytes.** (A) Diagram of KIF13B structure. KIF13B is composed of 1843 amino acids. Motor, motor domain; FHA, FHA domain, which binds to centaurin-α; MBS, MBS domain, which binds to hDLG1; CC, coiled-coil domains, whose functions have not yet been reported; CAP-Gly, a binding motif for the plus-ends of microtubules. (B) KIF13B is highly expressed in the liver. (a) Crude extracts of 11 kinds of tissues from adult mice (20 µg protein/lane) were subjected to immunoblotting analyses using antibodies against KIF13B and KIF5B. KIF5B, a conventional kinesin, was used as a reference. (b) Amounts of KIF13B and KIF5B in the tissues normalized by the corresponding amounts in the brain. (c) KIF13B/KIF5B ratios in the tissues normalized by the corresponding ratio in the brain. Br, brain; He, heart; Lu, lung; Sp, spleen; Li, liver; Ki, kidney; In, intestine; Mu, muscle; Te, testis; Ov, ovary; Ut, uterus. The data shown are from a single representative experiment out of four repeats. (C) KIF13B is located along the sinusoid of the liver. Livers from WT and KO mice were stained for KIF13B. Bar, 20 µm. (D and E) KIF13B is on the sinusoidal plasma membrane of hepatocytes. (D) WT liver was double stained for KIF13B (green) and actin (Alexa 568–phalloidin; red). Arrow, sinusoidal region; arrowhead, bile duct region; n, nucleus; s, sinusoid; a–b, line measured in E. Bar, 10 µm. (E) KIF13B and actin intensities measured along the a–b line in D. The peak signals of KIF13B (green arrows) were found inside those of actin (red arrows). (F) KIF13B is expressed in hepatocytes. Crude extracts of the liver and isolated hepatocytes (20 µg protein/lane) were subjected to immunoblotting analyses using antibodies against KIF13B, KIF5B, and albumin, a hepatocyte marker.

to hDLG1 and utrophin, which in turn bound to LRP1 and caveolae, respectively. These linkages were required for the KIF13B-enhanced endocytosis of LRP1. Therefore, we propose that KIF13B, working as a scaffold underneath the plasma membrane, enhances caveolin-dependent endocytosis of LRP1 by recruiting LRP1 to caveolae via LRP1–hDLG1–KIF13B–utrophin–caveolae linkage.

Results

KIF13B is localized on the sinusoidal plasma membrane of hepatocytes

To examine the physiological relevance of KIF13B in vivo, *kif13b*$^{-/-}$ (KO) mice were generated by gene targeting (Fig. 1 A; Fig. S1). KO mice were viable and fertile, with no gross anomalies and normal body size and weight (Fig. S1 F). Histological analyses on the major organs of the body did not show apparent changes between wild-type (WT) and knockout (KO) mice (Fig. S2).

We then searched for the tissues where KIF13B is abundantly expressed (Fig. 1 B). We evaluated a conventional kinesin, KIF5B, as a reference in this experiment, because KIF5B is the most abundant KIF and shows ubiquitous expression (Kanai et al., 2000; Hirokawa and Noda, 2008). Lung, liver, testis, ovary, and uterus showed high expression of KIF13B (more than four times higher than that in the brain; Fig. 1 B, a and b). Among them, liver exhibited the highest KIF13B/KIF5B ratio (more than four times higher than those in the other tissues examined, and in particular, 18 times higher than that in the brain; Fig. 1 B, c). Quantitative analyses revealed that KIF13B and

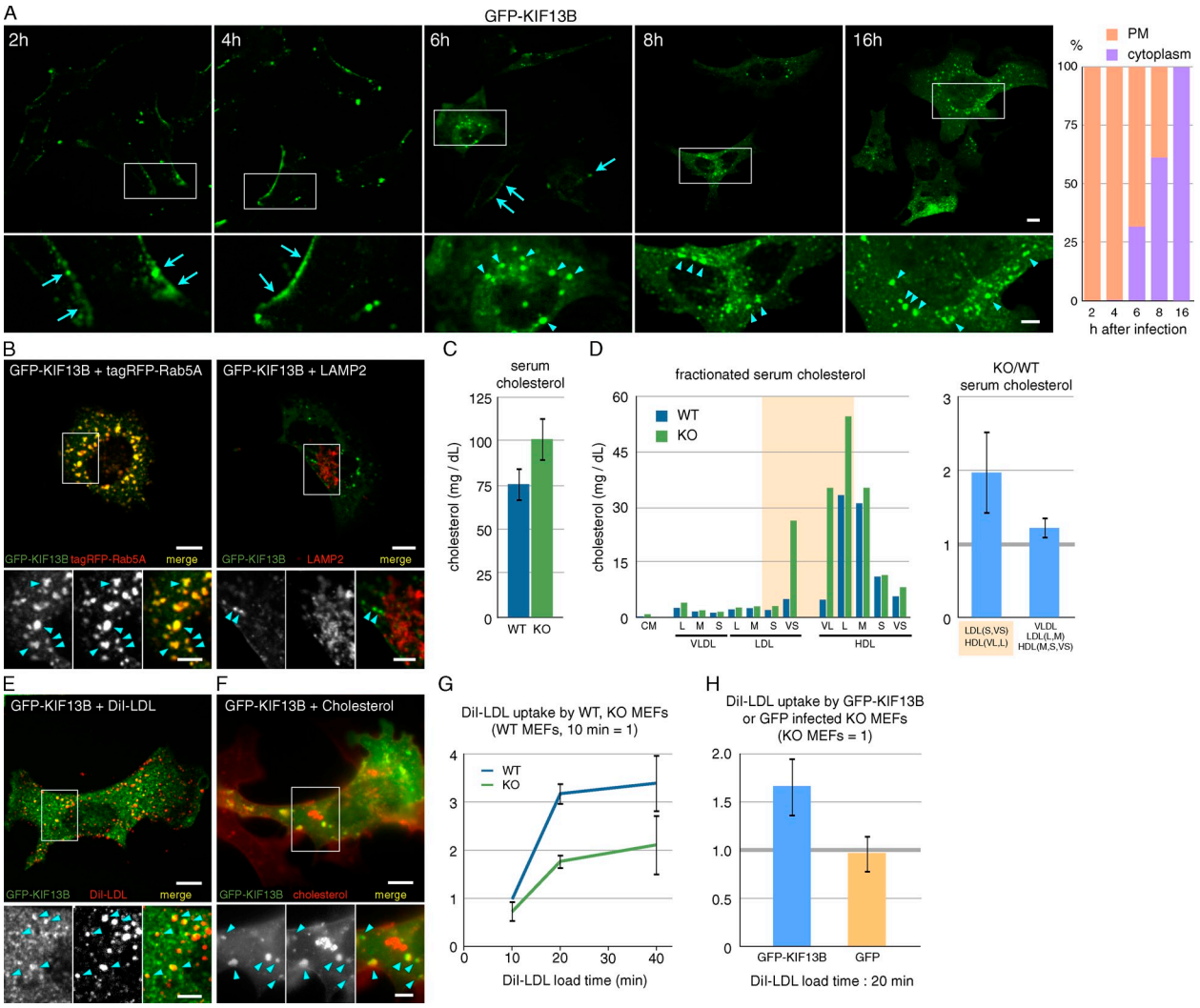

Figure 2. **KIF13B enhances the endocytosis of LDL.** (A) GFP-KIF13B, initially localized on the plasma membrane (2, 4, and 6 h; arrows), changes its localization to the cytoplasm in a vesicle-like structure with time (6, 8, and 16 h; arrowheads). (Left) KO MEFs were cultured for 2, 4, 6, 8, and 16 h after infection with GFP-KIF13B-adenovector. (Right) The ratio of the cells with GFP-KIF13B on the plasma membrane (PM) and exclusively on vesicles in the cytoplasm (n = 227–378 cells). (B) GFP-KIF13B–positive vesicles are early endosomes (arrowheads). KO MEFs transfected with GFP-KIF13B and tagRFP-Rab5A (an early endosome marker, left) or with GFP-KIF13B alone were cultured for 16 h. The latter were stained for LAMP2 (a late endosome marker, right). (C) Elevated serum cholesterol level in KO mice. The serum cholesterol levels in adult WT and KO mice were 75.5 ± 9.4 mg/dl and 101.1 ± 12.1 mg/dl, respectively (mean ± SD, n = 10 mouse pairs). (D) Cholesterol levels were elevated dominantly in small LDL and large HDL fractions in KO mice. (Left) A typical case of serum cholesterol profiles of WT and KO mice. (Right) KO/WT ratios of cholesterol in small LDL and large HDL fractions (colored fractions in the left panel) and in the remaining fractions were 1.97 ± 0.56 and 1.23 ± 0.14, respectively. (mean ± SD, n = 4 mouse pairs). VL, very large; L, large; M, medium; S, small; VS, very small. (E) KIF13B is associated with a subset of early endosomes containing newly endocytosed LDL. DiI-LDL was applied to GFP-KIF13B–transfected KO MEFs for 7 min before fixation. Arrowheads point to GFP-KIF13B/DiI-LDL double-positive vesicles. (F) KIF13B-associated vesicles are rich in cholesterol (arrowheads). KO MEFs transfected with GFP-KIF13B were stained with filipin, a cholesterol dye. 88.7 ± 6.7% of GFP-KIF13B–positive area was cholesterol positive (mean ± SD, n = 20 cells). (G) Decreased uptake of LDL in KO MEFs. DiI-LDL was applied to WT and KO MEFs for 10, 20, and 40 min. DiI intensities of endocytosed DiI-LDL were measured and normalized by that of the WT MEFs incubated for 10 min (mean ± SD, n = 4 independent experiments). (H) Elevated uptake of LDL in GFP-KIF13B–infected KO MEFs. KO MEFs were cultured for 6 h after infection with GFP-KIF13B- or GFP-adenovector. DiI-LDL was applied to the cells for 20 min and the DiI intensities of infected cells were compared with that of non-infected cells (GFP-KIF13B: 1.65 ± 0.30; GFP: 0.97 ± 0.19; mean ± SD, n = 4 independent experiments). The bottom panels show higher magnification images of the boxed areas. Bars: (main panels) 10 μm; (insets) 5 μm.

KIF5B comprised 0.072% and 0.053% of liver crude extract proteins, respectively (not depicted). This indicates that in the liver, KIF13B shows similarly high expression to the most abundant KIF, KIF5B.

KIF13B was observed along the sinusoid of the liver, where the sinusoidal plasma membrane of hepatocytes and the sinusoidal epithelial cells are separated by the space of Disse (Fig. 1 C). Because the space of Disse is filled with numerous actin-rich microvilli originating from hepatocytes, liver sections were stained for KIF13B and actin to determine the localization of KIF13B (Fig. 1, D and E). KIF13B was detected on the hepatocyte side of the actin-rich microvilli, indicating the localization of KIF13B on the sinusoidal plasma membrane of hepatocytes. The expression of KIF13B in hepatocytes was confirmed by immunoblotting analyses of isolated hepatocytes (Fig. 1 F).

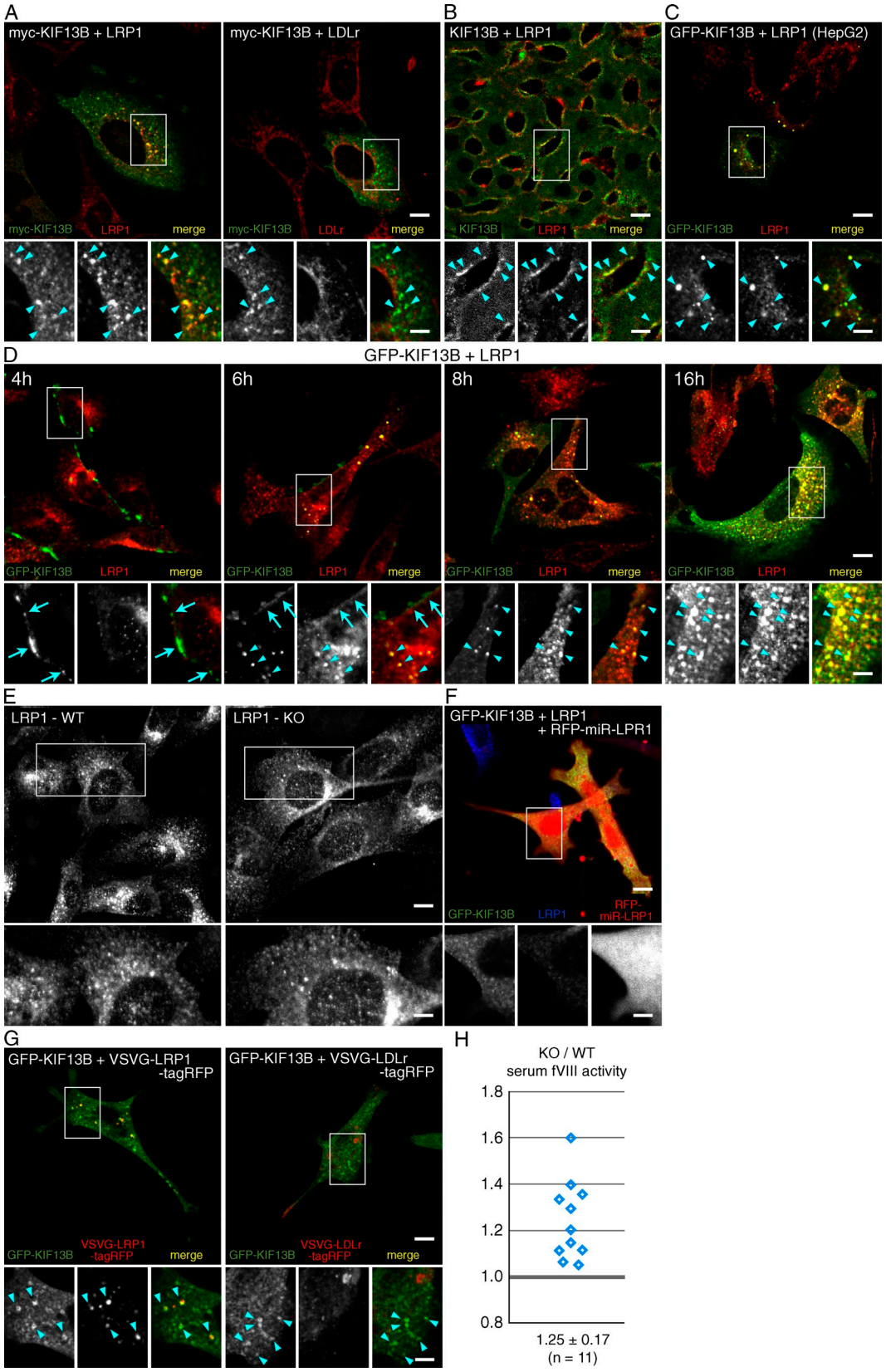

Figure 3. **KIF13B enhances LRP1-mediated endocytosis.** (A) KIF13B is associated with LRP1-containing vesicles (arrowheads). Myc-KIF13B-transfected KO MEFs were double stained for myc-tag and LRP1 (left) or LDLr (right). (B) KIF13B is colocalized with LRP1 on the sinusoidal plasma membrane of hepatocytes (arrowheads). WT liver was double stained for KIF13B and LRP1. (C) KIF13B is associated with LRP1-containing vesicles in cultured hepatic cells, HepG2 cells (arrowheads). HepG2 cells cultured for 16 h after infection with GFP-KIF13B-adenovector were stained for LRP1. (D) KIF13B translocates from the plasma membrane to the vesicles in the cytoplasm with LRP1. KO MEFs cultured for 4, 6, 8, and 16 h after infection with GFP-KIF13B-adenovector were stained for LRP1. (4 h) LRP1 was not associated with GFP-KIF13B on the plasma membrane. (6 h) LRP1 was associated with GFP-KIF13B both on the plasma

KIF13B enhances the endocytosis of LDL

To investigate the role of KIF13B at the cellular level, we established clonal mouse embryonic fibroblasts (MEFs) from WT and KO embryos. The expression of KIF13B in WT MEFs, but not in KO MEFs, was verified by immunoblotting (Fig. S3). We first examined the distribution of exogenous GFP-tagged KIF13B (GFP-KIF13B) in KO MEFs (Fig. 2 A). Cells were infected with GFP-KIF13B-adenovector and cultured for 2, 4, 6, 8, and 16 h. GFP-KIF13B was initially localized on the plasma membrane of the cells like intrinsic KIF13B in the liver (2 and 4 h). However, with time, distribution of GFP-KIF13B changed from the plasma membrane to the vesicles in the cytoplasm (6, 8, and 16 h). To confirm this translocation to be through endocytosis, we examined the relationship between KIF13B-positive vesicles and endosome markers, such as Rab5 (early endosome) and LAMP2 (late endosome). TagRFP-Rab5A was localized to GFP-KIF13B–positive vesicles in the cotransfected cells, whereas LAMP2 was not, indicating the vesicles to be early endosomes (Fig. 2 B). Association of KIF13B with the newly endocytosed LDL also confirmed that the KIF13B-positive vesicles were early endosomes (see below; Fig. 2 E).

Our data suggest that KIF13B is involved in endocytosis on the sinusoidal plasma membrane of hepatocytes. Because lipoproteins, especially small fractions of LDL and large fractions of high-density lipoprotein (HDL), are major targets of endocytosis in hepatocytes, we measured the serum cholesterol levels in WT and KO mice and found increased levels in KO mice (Fig. 2 C). We further analyzed the cholesterol profiles among the serum lipoproteins (Fig. 2 D). The KO/WT ratio of the cholesterol level in small fractions of LDL and large fractions of HDL (Fig. 2 D, colored fractions) was dominantly elevated compared with that in the other fractions. These data strengthen the potential role of KIF13B in cholesterol metabolism through the uptake of LDL/HDL in the liver.

We then investigated the role of KIF13B in the uptake of LDL at the cellular level. First, we examined the relationship between KIF13B-positive vesicles and endocytosed LDL. GFP-KIF13B–transfected KO MEFs were incubated with DiI-LDL for 7 min before fixation. Some, but not all, DiI-LDL–positive vesicles were GFP-KIF13B positive (Fig. 2 E). Because LDL is rich in cholesterol, we stained GFP-KIF13B–transfected KO MEFs with a cholesterol marker dye, filipin, and found GFP-KIF13B–positive vesicles to be rich in cholesterol (Fig. 2 F). These observations indicate the presence of an endocytic pathway for LDL that involves KIF13B.

Next, we investigated the effect of KIF13B on the uptake of LDL. WT and KO MEFs were incubated with DiI-LDL for 10, 20, and 40 min, and the intensity of endocytosed DiI-LDL was measured (Fig. 2 G). Uptake of DiI-LDL was decreased in KO MEFs at each incubation time. We then examined the uptake of LDL in the KO MEFs expressing exogenous KIF13B. KO MEFs and KO MEFs cultured for 6 h after infection with GFP-KIF13B- or GFP-adenovector were incubated with DiI-LDL for 20 min, and the intensity of endocytosed DiI-LDL was measured (Fig. 2 H). KO MEFs expressing GFP-KIF13B, but not GFP, showed elevated uptake of DiI-LDL compared with control KO MEFs. Therefore, we conclude that KIF13B enhances the endocytosis of LDL.

KIF13B enhances LRP1-mediated endocytosis

In mice, KIF13B was localized on the sinusoidal plasma membrane of hepatocytes, and KIF13B-deficient mice showed an elevated level of serum cholesterol. In cultured cells, KIF13B enhanced the endocytosis of LDL and was associated with LDL-containing early endosomes. We therefore investigated the relationship between KIF13B and receptors for LDL/HDL, such as LRP1 (Lillis et al., 2008) and LDL receptor (LDLr; Jeon and Blacklow, 2005). Expression of LRP1 and LDLr in MEFs and the liver was confirmed by immunoblotting (Fig. S3). We examined the distribution of LRP1 and LDLr in myc-tagged KIF13B (myc-KIF13B)-transfected KO MEFs (Fig. 3 A). Myc-KIF13B was localized to LRP1-containing but not LDLr-containing vesicles, and LRP1-containing vesicles were enlarged in the transfected cells (Fig. S4). KIF13B and LRP1 were colocalized on the sinusoidal plasma membrane of hepatocytes in the liver, and the localization of GFP-KIF13B to LRP1-containing vesicles was also observed in the human hepatic cell line, HepG2 (Fig. 3, B and C).

Because distribution of GFP-KIF13B changed with time (Fig. 2 A), we examined the localization of LRP1 in KO MEFs cultured for 4, 6, 8, and 16 h after infection with GFP-KIF13B-adenovector (Fig. 3 D). GFP-KIF13B was mostly localized on the plasma membrane of the cells cultured for 4 h after infection; however, LRP1 was not associated with GFP-KIF13B. With time, GFP-KIF13B translocated from the plasma membrane to vesicles in the cytoplasm, and LRP1 was associated with GFP-KIF13B both on the plasma membrane and on the endocytosed vesicles (6 h). The number of GFP-KIF13B/LRP1–positive vesicles in the cytoplasm increased with time (8 and 16 h). These data indicate that KIF13B is involved in LRP1-mediated endocytosis and is associated with LRP1-containing endosomes. A slight decrease in the size of LRP1-containing vesicles in KO MEFs was consistent with these observations (Fig. 3 E; Fig. S4).

membrane and on the vesicles in the cytoplasm. (8 and 16 h) GFP-KIF13B–associated, LRP1-containing vesicles increased with time. 77.4 ± 13.9% of GFP-KIF13B–positive area was LRP1 positive (8 h, mean ± SD, n = 21 cells). Arrows and arrowheads point to GFP-KIF13B on the plasma membrane and on the vesicles in the cytoplasm, respectively. (E) LRP1 vesicles in WT and KO MEFs. WT and KO MEFs were stained for LRP1. (F) Diffuse distribution of KIF13B in the LRP1-depleted cells. GFP-KIF13B was transfected to the KO MEFs with LRP1 knockdown by a tagRFP-miR-LRP1 vector. Two knockdown vectors showed similar results. (G) Association of KIF13B with LRP1-containing vesicles is through the cytoplasmic domain of LRP1 (arrowheads). KO MEFs were transfected with GFP-KIF13B and VSVG-LRP1-tagRFP (left) or VSVG-LDLr-tagRFP (right). (H) Elevated serum fVIII in the KO mice. KO/WT ratios of serum fVIII activity were measured (KO/WT of fVIII activity: 1.25 ± 0.17, mean ± SD, n = 11 mouse pairs). The bottom panels show higher magnification images of the boxed areas. Bars: (main panels) 10 µm; (insets) 5 µm.

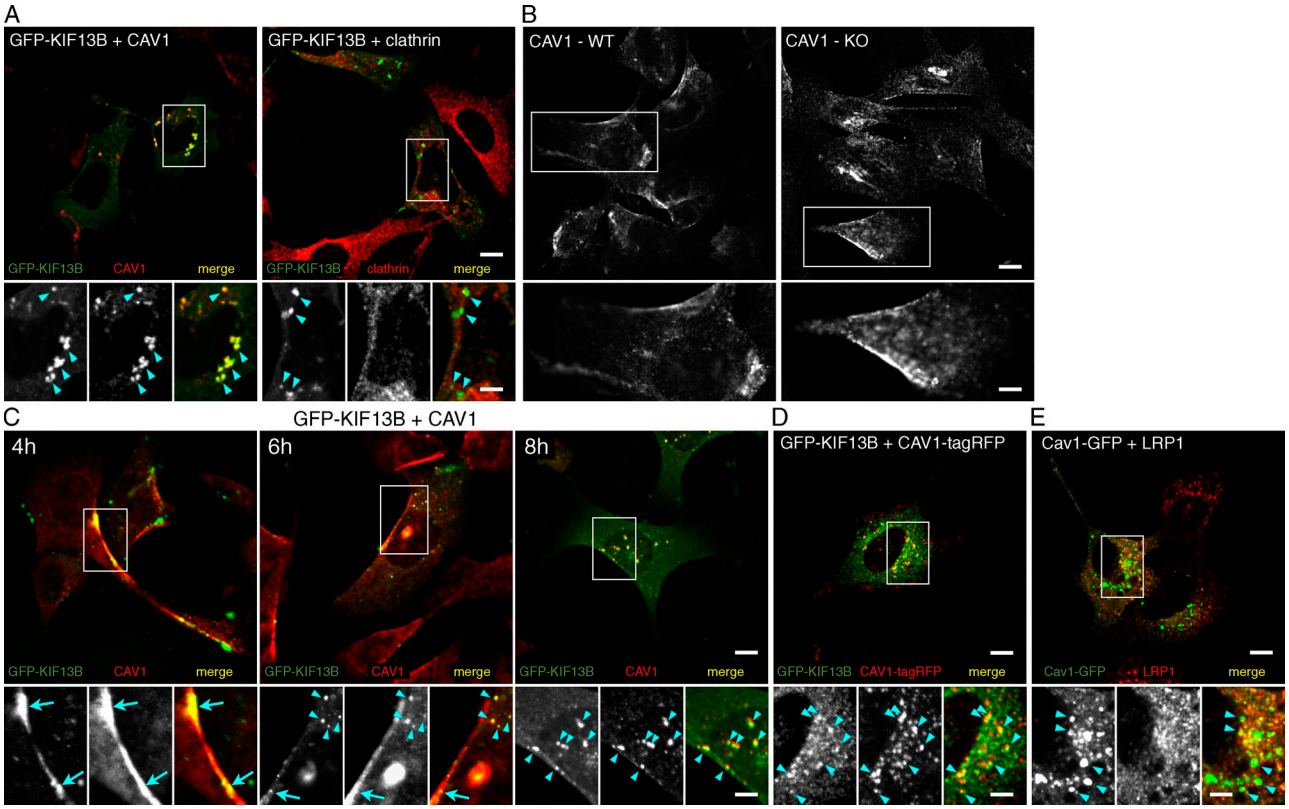

Figure 4. **KIF13B uses caveolin-dependent endocytic pathway.** (A) KIF13B-positive vesicles are associated with caveolin-1, but not with clathrin (arrowheads). GFP-KIF13B-transfected KO MEFs were stained for caveolin-1 (left) or clathrin (right). (B) Caveolin-1 in WT and KO MEFs. WT and KO MEFs were stained for caveolin-1. (C) KIF13B was colocalized with caveolin-1 both on the plasma membrane (arrows) and on the vesicles in the cytoplasm (arrowheads). KO MEFs cultured for 4, 6, and 8 h after infection with GFP-KIF13B-adenovector were stained for caveolin-1. 83.1 ± 13.5% of GFP-KIF13B–positive area was caveolin-1 positive (8 h, mean ± SD, *n* = 24 cells). (D) Caveolin-1-tagRFP was mostly colocalized to GFP-KIF13B in the co-transfected KO MEFs (arrowheads). 76.2 ± 13.4% of caveolin-1-tagRFP–positive area was GFP-KIF13B positive (mean ± SD, *n* = 33 cells). (E) "Caveosomes" generated by exogenous caveolin-1-GFP are distinct from LRP1-containing vesicles. KO MEFs transfected with caveolin-1-GFP were stained for LRP1. 21.1 ± 18.3% of caveolin-1-GFP–positive area was LRP1 positive (mean ± SD, *n* = 25 cells). The bottom panels show higher magnification images of the boxed areas. CAV1, caveolin-1. Bars: (main panels) 10 µm; (insets) 5 µm.

We then investigated the distribution of KIF13B in the LRP1 knockdown cells and found GFP-KIF13B to be diffusely distributed in the absence of LRP1 (Fig. 3 F). This suggests the specific association of KIF13B with LRP1-containing vesicles and the requirement of LRP1 for the KIF13B-enhanced endocytosis. The question then arose as to whether KIF13B binds to these vesicles through the cytoplasmic domain of LRP1. To address this question, GFP-KIF13B was transfected into KO MEFs with VSVG-LRP1-tagRFP or control VSVG-LDLr-tagRFP vector, which was composed of the extracellular domain of VSVG, the transmembrane and cytoplasmic domain of LRP1 or LDLr, and tagRFP (Fig. 3 G). GFP-KIF13B was localized to VSVG-LRP1-tagRFP–containing vesicles, but not to VSVG-LDLr-tagRFP–containing ones. These findings indicate that KIF13B is associated with LRP1-containing vesicles via the cytoplasmic domain of LRP1.

LRP1 is a multifunctional receptor that is known to bind to many different ligands (Lillis et al., 2008). fVIII is the one of the ligands specific for LRP1, and not LDLr (Lenting et al., 1999; Saenko et al., 1999). LRP1 polymorphisms influence the serum fVIII level in humans (Franchini and Montagnana, 2011), and mice with a liver-specific LRP1 deletion show an increased serum fVIII level (Bovenschen et al., 2003). Therefore, we analyzed the serum fVIII activity in WT and KO littermate mice (Fig. 3 H). Serum fVIII activity was higher in the KO mouse in every pair, suggesting a reduced function of LRP1 in the uptake of serum fVIII in KO mice. Therefore, we conclude that KIF13B enhances the endocytosis of LRP1, and that disruption of KIF13B decreases LRP1-mediated endocytosis.

KIF13B uses caveolin-dependent endocytic pathway

To find the endocytic pathway for the KIF13B-enhanced endocytosis of LRP1, we examined the distribution of caveolin-1 and clathrin in the GFP-KIF13B–transfected cells (Fig. 4 A). Caveolin-1, but not clathrin, was localized to GFP-KIF13B–positive vesicles, suggesting that KIF13B uses the caveolin-dependent pathway. Because caveolin-1 formed caveolae mainly along the edge of the plasma membrane of WT and KO MEFs (Fig. 4 B), we examined the distribution of caveolin-1 in the KO MEFs cultured for 4, 6, and 8 h after infection with GFP-KIF13B-adenovector (Fig. 4 C). Caveolin-1, initially localized with GFP-KIF13B on the plasma membrane (4 and 6 h), was translocated to the vesicles in the cytoplasm with GFP-KIF13B, and disappeared from the plasma membrane (6 and 8 h). These data indicate that KIF13B enhances the endocytosis of LRP1 via caveolae using the caveolin-dependent pathway.

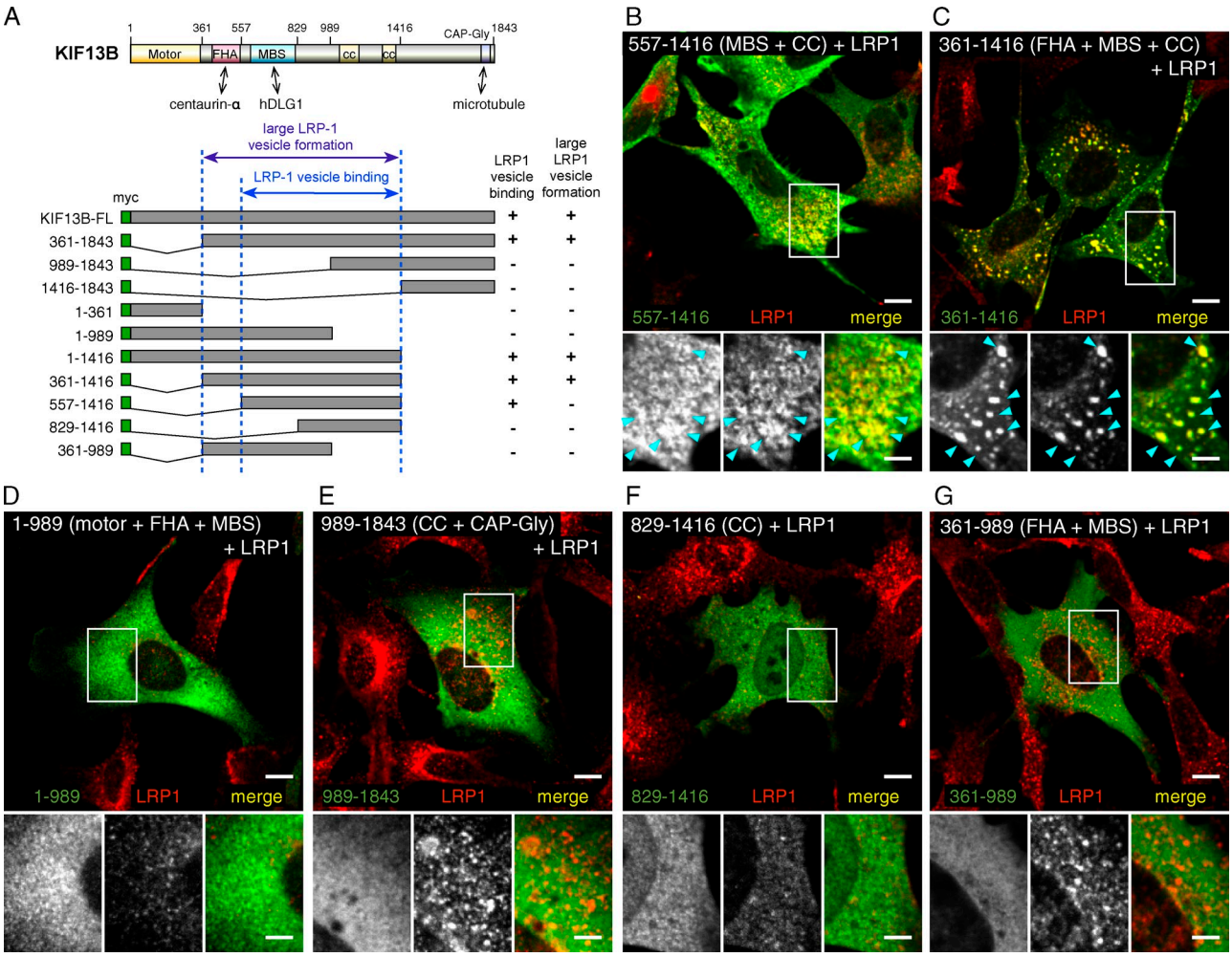

Figure 5. **KIF13B binds to LRP1-containing vesicles via the MBS and coiled-coil domains.** (A) Diagrams of the constructs for the myc-tagged KIF13B deletion mutants. The mutants were transfected to KO MEFs and their localization to LRP1-containing vesicles and large LRP1-containing vesicle formation were examined. "LRP1 vesicle binding": the KIF13B mutant was localized to LRP1-containing vesicles (+) or showed a diffuse distribution (−). "Large LRP1 vesicle formation": the size of LRP1-containing vesicles was enlarged (+) or was similar to those in the nontransfected cells (−). myc, myc-tag sequence. The numbers indicate the amino acid positions in KIF13B. (B–G) Representative images of immunofluorescence microscopy of KO MEFs transfected with myc-tagged KIF13B mutants, and stained for myc-tag and LRP1. The numbers represent the mutants shown in A and the labels (motor, FHA, MBS, CC, and CAP-Gly) indicate the domains included in the mutants. The MBS and CC domains were necessary for KIF13B to be associated with LRP1-containing vesicles (B, arrowheads). The FHA domain, together with the MBS and CC domains, was required for KIF13B to enlarge LRP1-containing vesicles. (C, arrowheads). Bars: (main panels) 10 µm; (insets) 5 µm.

We investigated the relationship between KIF13B, caveolin-1, and LRP1-containing vesicles. We first confirmed the localization of caveolin-1-tagRFP with GFP-KIF13B in the cotransfected cells (Fig. 4 D). We then examined the distribution of caveolin-1-GFP and LRP1-containing vesicles in the absence of KIF13B (Fig. 4 E). Caveolin-1-GFP induced caveolin-rich vesicles, "caveosomes," in the transfected KO MEFs (Hayer et al., 2010); however, the caveosomes were distinct from LRP1-containing vesicles. These data suggest that KIF13B is required for the recruitment of LRP1 to the caveolin-dependent endocytic pathway.

KIF13B binds to LRP1-containing vesicles via the MBS and coiled-coil domains

To solve the molecular mechanism of how KIF13B binds to LRP1-containing vesicles, we determined the region within KIF13B that was responsible for its binding to the vesicles. KIF13B is composed of motor, FHA, MBS, coiled-coil, and CAP-Gly domains (Fig. 5 A). The motor domain possesses motor activity, allowing KIF13B to travel along microtubules (Hirokawa et al., 2010). The FHA domain binds to centaurin-α1 to activate Arf6; this activation occurs through the inhibition of the Arf6-GAP activity of centaurin-α1 (Venkateswarlu et al., 2005). The MBS domain binds to hDLG1 (Hanada et al., 2000). The roles of the two coiled-coil domains remain unknown. The CAP-Gly domain binds to the plus-ends of microtubules (Steinmetz and Akhmanova, 2008). We designed a series of KIF13B deletion mutants and examined their binding to LRP1-containing vesicles (Fig. 5). The MBS and coiled-coil domains (557–1416) were sufficient for the localization of KIF13B to LRP1-containing vesicles (Fig. 5 B), and the FHA domain, together with the MBS and coiled-coil domains (361–1416), was required for KIF13B to enlarge LRP1-containing vesicles (Fig. 5 C). On the other hand, the mutants lacking either the

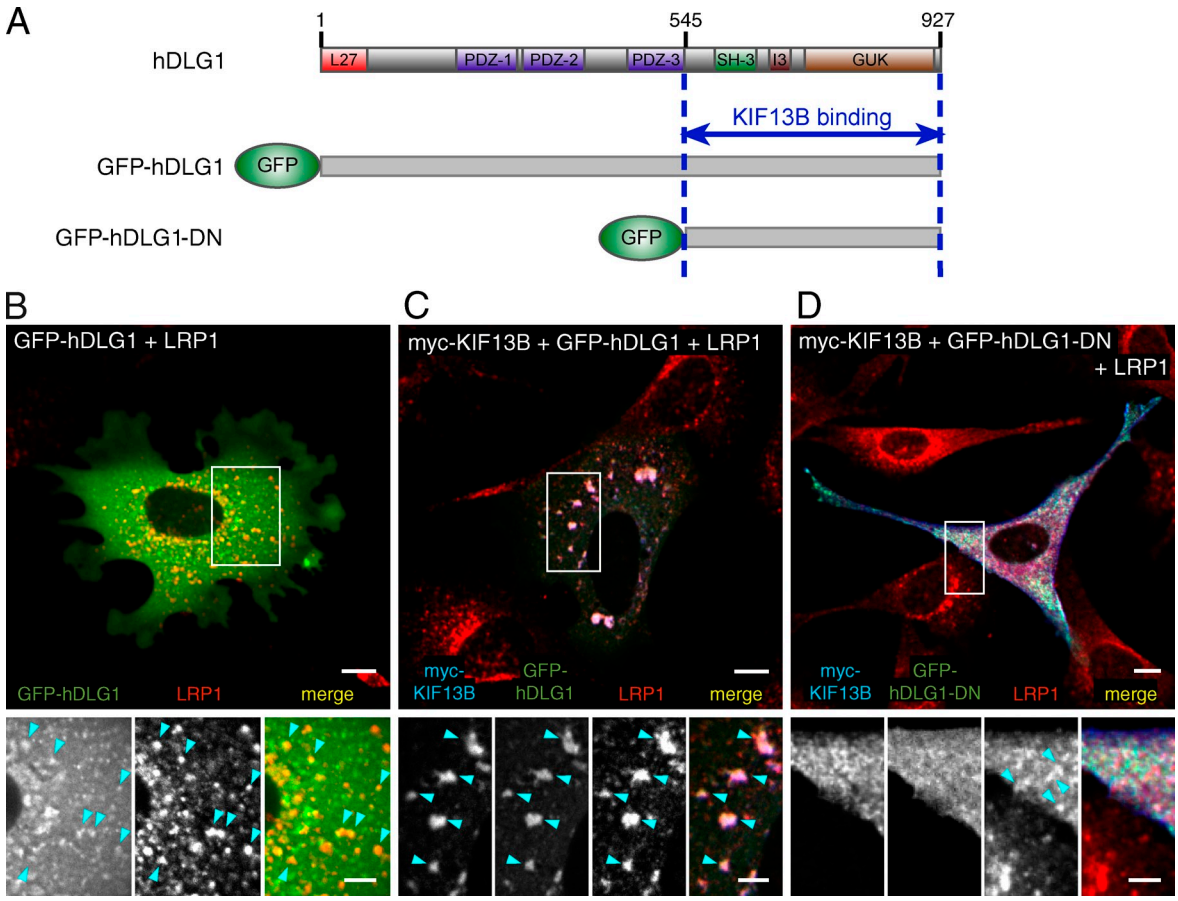

Figure 6. **hDLG1 links KIF13B to LRP1-containing vesicles.** (A) Diagrams of hDLG, GFP-hDLG1, and its dominant-negative mutant, GFP-hDLG1-DN. hDLG1 is composed of L27, PDZx3, SH-3, I3, and guanylate kinase homologue (GUK) domains. GFP-hDLG1-DN is composed of the binding domain of hDLG1 to KIF13B (Yamada et al., 2007). (B–D) hDLG1 links KIF13B to LRP1-containing vesicles. KO MEFs were transfected with GFP-hDLG1 alone (B), cotransfected with myc-KIF13B and GFP-hDLG1 (C), or GFP-hDLG1-DN (D). Transfected myc-KIF13B and intrinsic LRP1 were stained with anti-myc and anti-LRP1 antibodies, respectively. (B) GFP-hDLG1 was associated with LRP1-containing vesicles even in the absence of KIF13B, although the major part of GFP-hDLG1 remained in the cytoplasm. 58.9 ± 12.4% of GFP-hDLG1–positive area (vesicle) was LRP1 positive (mean ± SD, n = 27 cells). (C) Myc-KIF13B and GFP-hDLG1 were mostly localized to enlarged LRP1-containing vesicles. 89.9 ± 8.6% and 91.0 ± 9.0% of myc-KIF13B–positive areas were LRP1 and GFP-hDLG1 positive, respectively (mean ± SD, n = 24 cells). (D) Myc-KIF13B and GFP-hDLG1-DN showed diffuse distribution. The bottom panels show higher magnification images of the boxed areas. Arrowheads point to LRP1-containing vesicles in the transfected cells. Bars: (main panels) 10 µm; (insets) 5 µm.

MBS domain or the coiled-coil domains showed diffuse distribution in the cell (Fig. 5, D–G). These findings indicate that both the MBS and coiled-coil domains are necessary for KIF13B to be localized to LRP1-containing vesicles.

hDLG1 links KIF13B to LRP1-containing vesicles

To define the contributions of the MBS and coiled-coil domains to KIF13B localization in more detail, we examined each domain individually. First, we investigated the role of the MBS domain. Because KIF13B binds to hDLG1 through this domain (Hanada et al., 2000), we examined the role of hDLG1 in the KIF13B enhanced endocytosis of LRP1 (Fig. 6). When GFP-hDLG1 was expressed in KO MEFs, it was localized to LRP1-containing vesicles, but remained partially in the cytoplasm (Fig. 6 B). The size of the vesicles was similar to that in the nontransfected cells (Fig. S4). These observations indicate that hDLG1 can bind to LRP1-containing vesicles even in the absence of KIF13B, but is not enough to enhance the endocytosis of LRP1. To examine the relationship between KIF13B, hDLG1, and LRP1-containing vesicles, myc-KIF13B was transfected to KO MEFs with GFP-hDLG1 or a dominant-negative mutant, GFP-hDLG1-DN, composed of its KIF13B-binding region (Fig. 6, A, C, and D). Myc-KIF13B and GFP-hDLG1 cooperatively enhanced localization of each other to enlarged LRP1-containing vesicles (Fig. 6 C; Fig. S4). On the other hand, myc-KIF13B and GFP-hDLG1-DN showed diffuse distribution, and were not localized to LRP1-containing vesicles (Fig. 6 D). These findings indicate that hDLG1 links KIF13B to LRP1-containing vesicles, and that the recruitment of KIF13B to LRP1 is important for the enhanced endocytosis of LRP1.

Identification of utrophin as a binding partner of KIF13B

Next, we investigated the role of the coiled-coil domains. Because hDLG1 was observed not only on the sinusoidal but also on the basolateral plasma membranes of hepatocytes (Fig. 7 A), we assumed the presence of other factor(s), located on the

sinusoidal plasma membrane of hepatocytes, which bind to the C-terminal region of KIF13B including the coiled-coil domains.

We first examined the binding between the coiled-coil domains of KIF13B (829–1416) and the cytoplasmic domain of LRP1 (4445–4544) using yeast two-hybrid experiments, but could not detect any interaction between these proteins (unpublished data). We then searched for binding partners of KIF13B using immunoprecipitation experiments (Fig. 7 B). A 400-kD band was coprecipitated with KIF13B in a WT-specific manner, and was identified as utrophin (Tinsley et al., 1992; Guo et al., 1996). Utrophin was expressed in MEFs and the liver (Fig. S3), and was localized on the sinusoidal plasma membrane of hepatocytes (Fig. 7 C), as previously reported (Takahashi et al., 2005). Utrophin is composed of a calponin homology (CH) domain, 22 spectrin repeats, a WW domain, two EF hand regions, and a ZZ domain zinc finger (Fig. 6 D; Haenggi and Fritschy, 2006). Utrophin is a component of dystrophin–dystroglycan complex (Haenggi and Fritschy, 2006). The CH domain binds to the actin cytoskeleton. The WW domain binds to βDG, which is localized along the sinusoidal plasma membrane of hepatocytes (Durbeej et al., 1998). Utrophin complex interacts with caveolin-1 in caveolae (Ramírez-Sánchez et al., 2012) and utrophin competes with caveolin for the binding to βDG (Sotgia et al., 2000; Ilsley et al., 2002).

We then searched for the binding domains between KIF13B and utrophin using deletion mutants. First, we determined the KIF13B-binding domain on utrophin using myc-tagged full-length KIF13B and a series of FLAG-tagged utrophin mutants (Fig. 7 D). Only the mutants containing the N-terminal region of utrophin (1–1098) were able to bind to KIF13B. Therefore, this region was defined as the KIF13B-binding domain on utrophin, and was used to determine the utrophin-binding domain on KIF13B (Fig. 7 E), and to create dominant-negative mutants of utrophin (FLAG-Utrn-DN and Utrn-DN-GFP). Next, we determined the utrophin-binding domain on KIF13B using FLAG-tagged utrophin (1–1098) and a series of myc-tagged KIF13B mutants (Fig. 7 E). Utrophin (1–1098) bound to the C-terminal region of KIF13B, which included the coiled-coil domains (989–1843).

Because KIF13B binds to hDLG1 and utrophin through the different domains, they can form hDLG1–KIF13B–utrophin complex. To examine the presence of this complex in vivo, we performed an immunoprecipitation experiment using WT and KO mouse livers (Fig. 7 F). KIF13B, hDLG1, and utrophin were coprecipitated from WT mouse liver. This WT-specific co-precipitation of hDLG1 and utrophin clearly indicates the KIF13B-mediated linkage between utrophin and hDLG1. Because hDLG1 recruited KIF13B to LRP1-containing vesicles (Fig. 6), KIF13B and hDLG1 can, in turn, recruit utrophin to the vesicles. We performed a series of transfection studies using FLAG-utrophin, GFP-KIF13B, and hDLG1 (Fig. 7, G–I). In the absence of KIF13B, FLAG-utrophin was not localized to LRP1-containing vesicles, but was diffusely distributed (Fig. 7 G). On the other hand, FLAG-utrophin was localized to GFP-KIF13B/LRP1–containing vesicles when GFP-KIF13B was cotransfected with FLAG-utrophin (Fig. 7 H). FLAG-utrophin was also localized to enlarged GFP-KIF13B/hDLG1/LRP1–containing vesicles in the cells cotransfected with FLAG-utrophin, GFP-KIF13B, and hDLG1 (Figs. 6 C and 7 I). These data confirmed the recruitment of utrophin to LRP1-containing vesicles via the LRP1–hDLG1–KIF13B–utrophin linkage at the cellular level.

Utrophin was located on the sinusoidal plasma membrane of hepatocytes, bound to the C-terminal region of KIF13B including the coiled-coil domains, and formed LRP1–hDLG1–KIF13B–utrophin linkage. Therefore, we conclude that utrophin is the factor that we assumed to be responsible for localizing KIF13B to LRP1-containing vesicles with hDLG1.

Utrophin links KIF13B to caveolae

Utrophin complex interacts with caveolin-1 in caveolae (Ramírez-Sánchez et al., 2012), and utrophin competes with caveolin for binding to βDG (Sotgia et al., 2000; Ilsley et al., 2002). Given the recruitment of utrophin to LRP1 via LRP1–hDLG1–KIF13B–utrophin linkage and the association of KIF13B with caveolae on the plasma membrane and with LRP1/caveolin-1–containing endosomes (Figs. 3 D and 4 C), utrophin may play an important role in the recruitment of LRP1 to caveolae.

First, we examined the role of utrophin in the linkage between KIF13B and caveolae. For this purpose, we blocked the binding between KIF13B and intrinsic utrophin using FLAG-Utrn-DN, a dominant-negative mutant of utrophin composed of its KIF13B binding domain (Fig. 7 D). To keep a sufficient amount of FLAG-Utrn-DN during the expression of GFP-KIF13B, KO MEFs were transfected with FLAG-Utrn-DN and cultured for 8 h before being infected with GFP-KIF13B-adenovector and cultured for additional 4 h (Fig. 7 J). GFP-KIF13B was observed on the plasma membrane even in the expression of FLAG-Utrn-DN; however, localization of caveolae to GFP-KIF13B was disrupted. Caveolae were localized to GFP-KIF13B in the control cells, such as FLAG-Utrn-DN–nonexpressing cells and control tagRFP-expressing cells (unpublished data). Therefore, utrophin plays an important role in the linkage between KIF13B and caveolae.

Next, to investigate the effect of loss of the linkage between KIF13B and caveolae in the endocytosis of LRP1, Utrn-DN-GFP was transfected with GFP-KIF13B and hDLG1 (Fig. 7 K, also refer to panel I). Despite the coexpression of hDLG1, the size of LRP1-containing vesicles was not enlarged (Fig. S4), although Utrn-DN-GFP and GFP-KIF13B were associated with the vesicles. Thus, utrophin-mediated linkage between KIF13B and caveolae was required for the KIF13B-enhanced caveolin-dependent endocytosis of LRP1. Taken together, the data from our present study collectively conclude that KIF13B enhances caveolin-dependent endocytosis of LRP1 through the recruitment of LRP1 to caveolae via LRP1–hDLG1–KIF13B–utrophin–caveolae linkage.

Discussion

In this study, we show that KIF13B enhances caveolin-dependent endocytosis of LRP1 by recruiting LRP1 to caveolae through the LRP1–hDLG1–KIF13B–utrophin–caveolae linkage (Fig. 8 A). KIF13B binds to hDLG1 and utrophin via the MBS domain and the C-terminal region containing the coiled-coil domains,

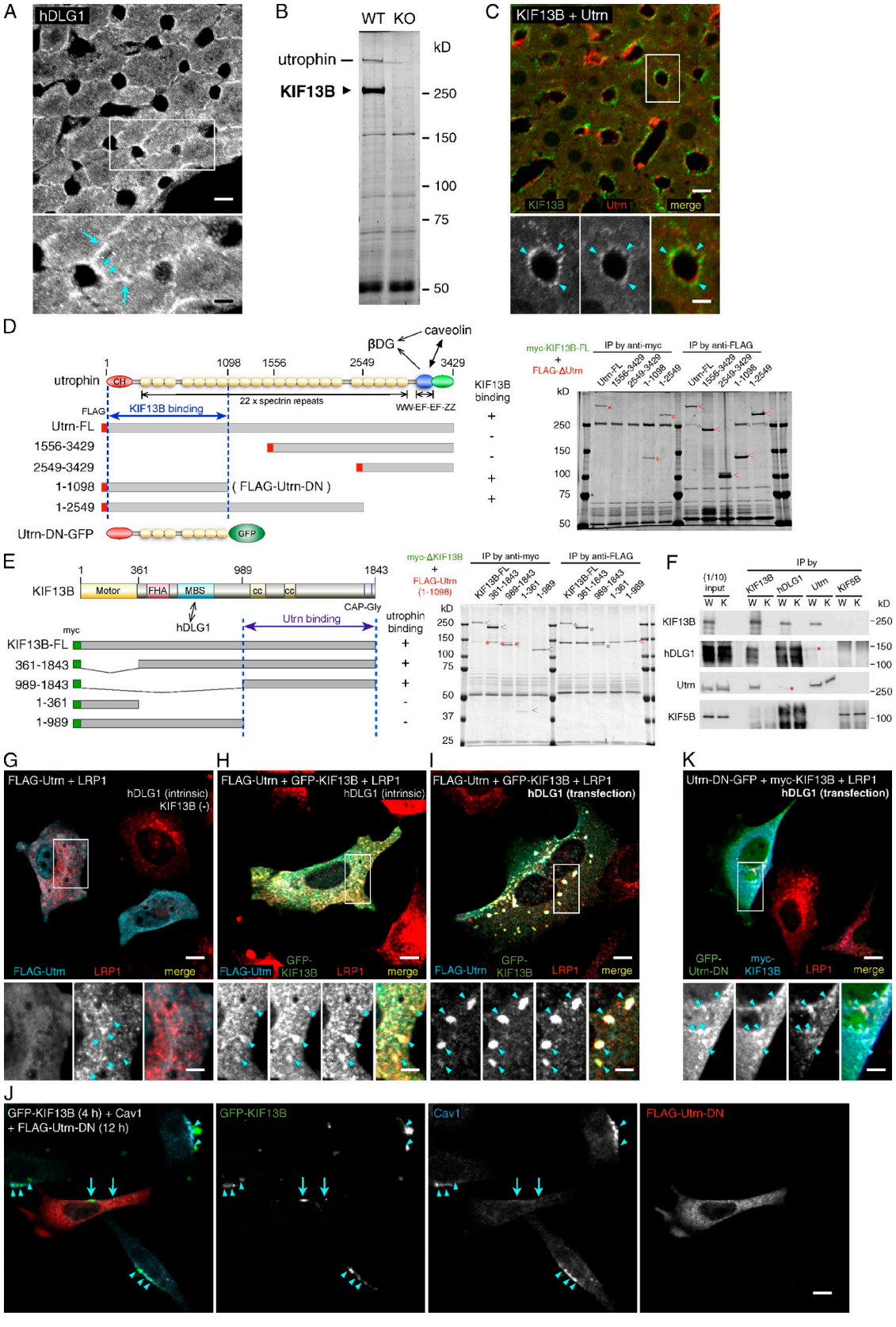

Figure 7. **Utrophin, a new KIF13B binding protein, links KIF13B to caveolae.** (A) hDLG1 is located on the sinusoidal (arrowheads) and basolateral (arrows) plasma membranes of hepatocytes. WT liver was stained for hDLG1. (B) Identification of utrophin as a new binding protein for KIF13B. WT and KO mouse liver homogenates were subjected to immunoprecipitation using an anti-KIF13B antibody. (C) Utrophin (Utrn) colocalized with KIF13B on the sinusoidal plasma membrane of hepatocytes (arrowheads). WT liver was double stained for KIF13B and utrophin. (D) N-terminal region of utrophin (1–1098) binds to KIF13B. Diagrams of the constructs for the FLAG-tagged utrophin mutants. Utrn (1–1098) was used to determine the utrophin-binding domain on KIF13B

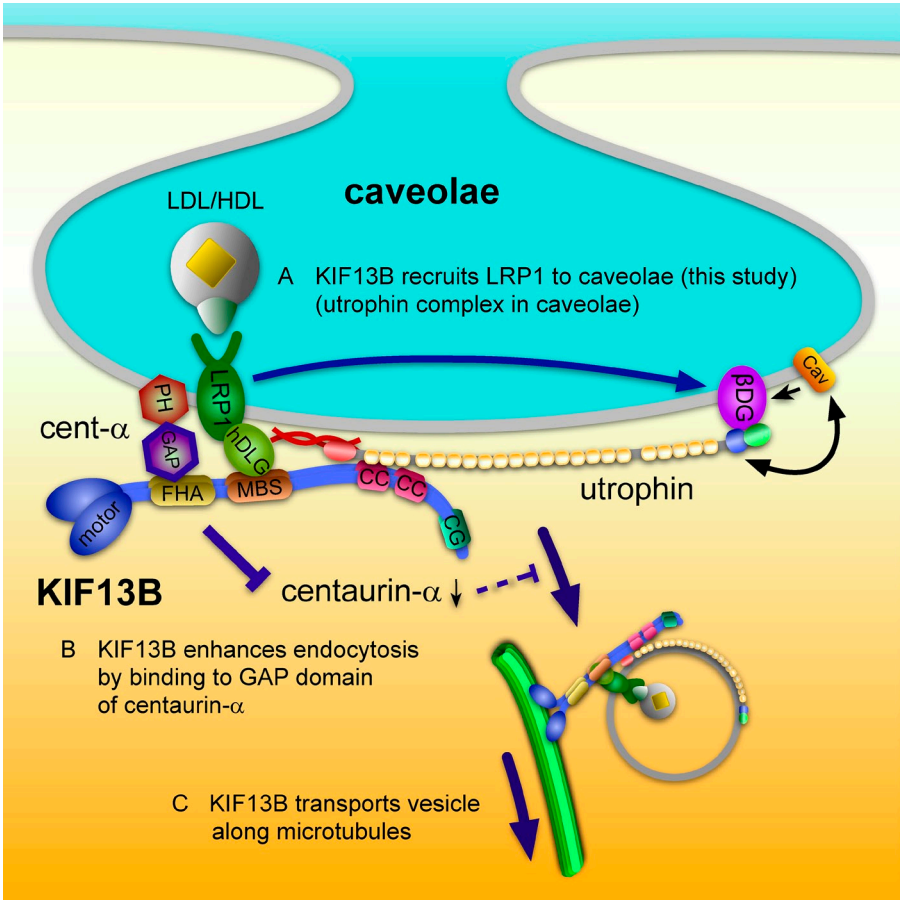

Figure 8. **Proposed model for the role of KIF13B in caveolin-dependent endocytosis of LRP1.** (A) KIF13B links LRP1 to caveolae through the LRP1–hDLG1–KIF13B–utrophin–caveolae linkage (this study). Utrophin complex interacts with caveolin-1 in caveolae (Ramírez-Sánchez et al., 2012) and utrophin competes with caveolin for the binding to βDG (Sotgia et al., 2000; Ilsley et al., 2002). (B) KIF13B activates Arf6 through the inhibition of Arf6-GAP activity of centaurin-α1, subsequently enhancing the endocytosis nearby (Venkateswarlu et al., 2005). (C) KIF13B, as a motor protein, transports the endocytosed vesicles along microtubules (Horiguchi et al., 2006; Hirokawa et al., 2010).

respectively (Fig. 7 E; Hanada et al., 2000). hDLG1 and utrophin, in turn, bind to LRP1-containing vesicles and caveolae, respectively (Figs. 6 and 7).

In addition to the MBS and the coiled-coil domains, the FHA domain was required for KIF13B to enlarge LRP1-containing vesicles (Fig. 5). The FHA domain binds to the GAP domain of centaurin-α1 (Venkateswarlu et al., 2005). Centaurin-α1 is composed of PH and GAP domains. The PH domain binds to PIP_3 and the GAP domain inactivates Arf6 (Czech, 2000; Venkateswarlu et al., 2007). Arf6 influences membrane trafficking and the functions of the actin cytoskeleton at the plasma membrane, such as endocytosis, exocytosis, and cell spreading (Donaldson, 2003). KIF13B inhibits the Arf6-GAP activity of centaurin-α1 and activates Arf6 (Venkateswarlu et al., 2005). Therefore, we predict that centaurin-α1, which is recruited to the plasma membrane upon PIP_3 generation by PI-3-kinase, inactivates adjacent Arf6; however, KIF13B binds to the GAP domain of centaurin-α1 to mask its activity, thereby

in E and to generate dominant-negative mutants (FLAG-Utrn-DN and Utrn-DN-GFP). "KIF13B binding": the utrophin mutant was coprecipitated with myc-KIF13B (+) or not (−). CH, calponin homology domain, an actin-binding motif; WW, WW domain; EF, EF hand region; ZZ, ZZ domain zinc finger; FLAG, FLAG-tag sequence. (E) C-terminal region of KIF13B binds to utrophin. Diagrams of the constructs for the myc-tagged KIF13B mutants. "Utrophin binding": the KIF13B mutant was coprecipitated with FLAG-Utrn (1–1098) (+) or not (−). In D and E, the numbers indicate the amino acid positions in utrophin and KIF13B, and the symbols "<" and "*" in the right panels indicate immunoprecipitated and coprecipitated proteins, respectively (green, myc-KIF13B mutants; red, FLAG-Utrn mutants). (F) KIF13B links utrophin and hDLG1. Immunoprecipitation from WT and KO mouse liver homogenates using antibodies against KIF13B, hDLG1, utrophin, and KIF5B (control). hDLG1 and utrophin were coprecipitated in a WT-specific manner (*). (G–I) KIF13B links utrophin to LRP1-containing vesicles via hDLG1. KO MEFs were transfected with FLAG-Utrn alone (G), with FLAG-Utrn and GFP-KIF13B (H), and with FLAG-Utrn, GFP-KIF13B, and hDLG1 (I). (G) FLAG-Utrn showed diffuse distribution in the absence of KIF13B. (H) FLAG-Utrn and GFP-KIF13B were colocalized on LRP1-containing vesicles. 84.3 ± 9.8% and 85.5 ± 15.5% of GFP-KIF13B–positive areas were LRP1 and FLAG-Utrn positive, respectively (mean ± SD, n = 25 cells). (I) FLAG-Utrn and GFP-KIF13B were colocalized on enlarged LRP1-containing vesicles under the coexpression of exogenous hDLG1. 83.0 ± 11.4% and 93.6 ± 7.2% of GFP-KIF13B–positive areas were LRP1 and FLAG-Utrn positive, respectively (mean ± SD, n = 25 cells). (J) Utrophin links KIF13B to caveolae. KO MEFs, cultured for 8 h after transfection with FLAG-Utrn-DN, were infected with GFP-KIF13B-adenovector and cultured for an additional 4 h. Localization of caveolae to GFP-KIF13B on the plasma membrane was disrupted in the FLAG-Utrn-DN–expressed cells (arrows), whereas caveolae were localized to GFP-KIF13B in the nonexpressed cells (arrowheads) or in the control tagRFP-expressed cells (not depicted). (K) Utrophin is required for the enhanced endocytosis of LRP1. KO MEFs were transfected with Utrn-DN-GFP, myc-KIF13B, and hDLG1. Utrn-DN-GFP and myc-KIF13B were colocalized on LRP1-containing vesicles; however, LRP1-containing vesicles were not enlarged even under the coexpression of exogenous hDLG1. 62.3 ± 17.2% and 64.4 ± 20.1% of myc-KIF13B–positive areas were LRP1 and Utrn-DN-GFP positive, respectively (mean ± SD, n = 24 cells). (G–K) FLAG-Utrn/Utrn-DN, myc-KIF13B, intrinsic LRP1, and intrinsic caveolin-1 were stained with antibodies against FLAG, myc, LRP1, and caveolin-1, respectively. Arrowheads point to LRP1-containing vesicles in the transfected cells (G–I and K). The bottom panels show higher magnification images of the boxed areas. Bars: (main panels) 10 µm; (insets) 5 µm.

allowing Arf6 to proceed with the endocytosis nearby (Fig. 8 B). After endocytosis, KIF13B would transport the endocytosed vesicle along microtubules as a motor protein (Fig. 8 C).

Caveolin-1 was located along the edge of the plasma membrane of WT and KO MEFs (Fig. 4 B); however, it showed focal distribution on the plasma membrane with exogenous KIF13B (Fig. 4 C, 4 h). Focal distribution of KIF13B was observed even when the linkage between KIF13B and caveolae was disrupted (Fig. 7 K). These results indicate that KIF13B is primarily localized focally on the plasma membrane, to which caveolae migrate.

LRP1 was not localized to KIF13B/caveolae on the plasma membrane in the cells cultured for 4 h after infection (Fig. 3 D; Fig. 4 C, 4 h). With time, LRP1 became localized to KIF13B/caveolae (Fig. 3 D; Fig. 4 C, 6 h) and was translocated to the vesicles in the cytoplasm with KIF13B and caveolin-1 (Fig. 3 D; Fig. 4 C, 6 h and 8 h). Given the requirement of LRP1 for the formation of KIF13B-positive vesicles (FIg. 3 F), recruitment of LRP1 to KIF13B/caveolae is a key event in the progression of endocytosis. The activity of PI-3-kinase is required for the insulin-stimulated migration of LRP1 to caveolae in adipocytes (Zhang et al., 2004). Because the activation of PI-3-kinase also drives FHA–centaurin-α1–Arf6–endocytosis cascade as discussed above, the precise molecular mechanism of how the FHA domain, together with PI-3-kinase, is involved in the KIF13B-enhanced endocytosis of LRP1 should be investigated in future studies.

The effect of the loss of KIF13B on the uptake of LDL was limited (Fig. 2 G, uptake of LDL by KO MEFs was ∼60% of that of WT). LRP1 uses the clathrin-dependent endocytic pathway in addition to the caveolin-dependent one (Zhang et al., 2004), and there are other receptors for LDL, such as LDLr. Indeed, KIF13B was not associated with a portion of early endosomes containing LDL (Fig. 2 E). Therefore, we conclude that LDL is also endocytosed through KIF13B-independent pathways, especially in the absence of KIF13B.

Certain kinds of receptors are endocytosed via the caveolin-dependent pathway (Pelkmans and Helenius, 2002). KIF13B is expressed ubiquitously (Fig. 1 A), but there are several hDLG1-like proteins, e.g., hDLG1 to hDLG4, which show distinct tissue distributions and interact with kinds of receptors (Fujita and Kurachi, 2000; Anderson and Grant, 2006; Hsueh, 2006). Therefore, a general mechanism could be possible, whereby KIF13B works as a scaffold protein that links receptors to the caveolin-dependent endocytic pathway in combination with their corresponding hDLG1-like proteins.

In contrast to piles of information about clathrin-dependent endocytosis, little is known about how caveolin-dependent endocytosis is regulated. This is the first demonstration of a molecular mechanism where a receptor is recruited to caveolae and endocytosed through the caveolin-dependent pathway.

Materials and methods

Clones and transfection

A KIF13B cDNA was cloned from a mouse brain cDNA library. VSVG-LRP1-tagRFP and VSVG-LDLr-tagRFP were constructed using VSVG (Nakata and Hirokawa, 2003), partial LRP1 (FANTOM 3 B930091M07), and full-length LDLr (FANTOM 3 G530109H06) clones. An hDLG1[I3] cDNA was constructed using FANTOM 3 clones (full-length hDLG1[I2]: F430107E01; partial hDLG1[I3]: 3830420N02). A caveolin-1 cDNA was constructed using a FANTOM 3 clone (9530073F05). A utrophin cDNA was a gift from J.M. Ervasti (University of Minnesota, Minneapolis, MN; Guo et al., 1996). The deletion mutants were constructed by restriction enzyme digestion or PCR. These cDNAs were confirmed by sequencing, and were tagged with GFP (Takara Bio Inc.), tagRFP (Evrogen), and myc (MEQKLISEEDL) sequences. GFP-KIF13B-adenovector was generated using the ViraPower adenoviral expression system (Invitrogen) according to the manufacturer's protocol. Cells were transfected using Lipofectamine 2000 (Invitrogen) or infected with GFP-KIF13B-adenovector according to the manufacturer's protocol. Transfected cells were cultured for 16 h before observation, unless otherwise noted. Infected cells were cultured for 2–16 h before observation.

Antibodies

An anti-KIF13B polyclonal antibody was produced by immunizing rabbits with a purified GST-tagged C-terminal KIF13B protein (1382–1843) expressed in BL21(DE3) *Escherichia coli* using the pGEX-4T-3 vector (GE Healthcare). The GST tag was removed from the protein by thrombin digestion before immunization. The antiserum was affinity purified using the antigen coupled to CNBr-activated Sepharose 4B beads (GE Healthcare). A rabbit polyclonal anti-KIF5B antibody, generated against the C-terminal sequence of KIF5B, was described previously (Kanai et al., 2000). Goat polyclonal anti-albumin (Bethyl Laboratories, Inc.), rat monoclonal anti-LAMP2 (ABL-93; Santa Cruz Biotechnology, Inc.), rabbit monoclonal anti-LRP1 (EPR3724; Abcam), rabbit monoclonal anti-LDLr (EP1553Y; Abcam), rabbit polyclonal anti-caveolin (sc-894; Santa Cruz Biotechnology, Inc.), mouse monoclonal anti-clathrin heavy chain (clone 23; BD), rabbit polyclonal anti-hDLG1 (sc-25661; Santa Cruz Biotechnology, Inc.), mouse monoclonal anti-utrophin (20C5, Abcam; 8A4, Santa Cruz Biotechnology, Inc.), mouse monoclonal anti-myc (9B11; Cell Signaling Technology), and mouse monoclonal anti-FLAG (M2; Sigma-Aldrich) primary antibodies were purchased commercially. Alexa Fluor–conjugated secondary antibodies and Alexa Fluor 568–conjugated phalloidin were purchased from Invitrogen.

Gene targeting of *kif13b*

A 13.5-kb genomic clone was isolated from a λEMBL3 genomic library of the embryonic stem (ES) cell line CMT1-1 using standard procedures (Kanai et al., 2000). A targeting vector was constructed using a promoter-trap strategy, and three loxP elements were inserted among the following four parts: (1) a 2-kb 5′ homologous region (short arm); (2) a 2.3-kb region (middle arm) containing the ATP-binding motif P-loop exon (p) and its upstream exon (p-1); (3) a newly introduced SA-IRES-βgeo-polyA cassette; and (4) a 9-kb 3′ homologous region (long arm).

The targeting vector was linearized by NotI digestion and electroporated into the ES cells. The homologous recombinant ES clones were isolated, and injected into blastocysts as described previously (Kanai et al., 2000). The chimeric mice were bred to C57BL/6J females, and the transmission of the neo allele to the agouti offspring was examined by PCR using the primer set of neoF (5′-TGGGCACAACAGACAATCGG-3′) and neoR (5′-ACTTCGCCCAATAGCAGCCAG-3′). *Kif13b*$^{3loxp/+}$ mice were mated with CAG-Cre mice to remove the p and p-1 exons together with the IRES-βgeo-polyA cassette to obtain KO mice. The mice were maintained by backcrossing with C57BL/6J mice for more than 10 generations in a specific pathogen-free environment. We determined the genotypes of the mice by PCR with primer sets p1 (5′-TTTAGCTCAGTGGCAGAGTGCTC-3′) and p2 (5′-ACACACCTGACCATGTTTGGG-3′) for the WT allele, and p1 and p3 (5′-TCACTGATCCATCTCTCCAGCACC-3′) for the KO allele. We used male mice to investigate the liver function to avoid the effects of pregnancy in this study.

Histological analyses

Mice were anesthetized and fixed by perfusion with 4% paraformaldehyde in PBS. Tissues were dissected out and fixed with 10% formalin. The tissues were then dehydrated in ethanol, embedded in paraffin, sectioned serially at 7-µm thickness using a microtome (model HM355; Rotary Microtome), and subjected to hematoxylin/eosin or Bodian staining according to standard methods. The stained sections were observed using an Axiophot light microscope (Carl Zeiss) equipped with a digital camera (model DXM1200; Nikon).

Hepatocyte isolation

The hepatocytes from 8-wk-old male mice were isolated using hepatocyte media (Gibco) according to the manufacturer's protocol. Isolated hepatocytes were subjected to immunoblotting analyses.

Establishment of immortalized MEFs

Primary MEFs were obtained from WT and KO mice at E13.5. For immortalization with the SV40 large T antigen, the cells were transfected with the pSV3hyg vector (Ueno et al., 2011) using the Effectene transfection reagent (QIAGEN) according to the manufacturer's protocol, and then subcloned in the presence of 200 µg/ml hygromycin B (Invitrogen). The transformed clones were maintained in high-glucose DMEM (Gibco) supplemented with 10% FCS at 37°C in a humidified 5% CO_2 atmosphere.

RNA interference (RNAi)

A BLOCK-iT Pol II miR RNAi expression kit (Invitrogen) was used according to the manufacturer's protocol. Four miRNAs for LRP1 were designed by BLOCK-iT RNAi Designer (https://rnaidesigner.lifetechnologies.com/rnaiexpress) based on the mouse LRP1 sequence (GenBank/EMBL/DDBJ accession no.: NM_008512). As a marker, tagRFP was inserted into the DraI–SalI sites of the vectors. The knockdown vectors were transfected into *kif13b* KO MEFs. At 12 h after transfection, the medium was replaced and the cells were incubated for another 48 h. The cells were then used for transfection experiments with GFP-KIF13B. Knockdown of intrinsic LRP1 was confirmed by immunofluorescence microscopy using an anti-LRP1 antibody. Two of the miRNA vectors successfully suppressed intrinsic LRP1 and showed same results. Their inserted sequences were 5′-TGCTGTAAAGATTGTCTCCCATCCAGGTTTTGGCCACTGACTGACCTGGATGGGACAATCTTTA-3′ and 5′-TGCTGTTAAGCTGAACACCAATGCCTGTTTTGGCCACTGACTGACAGGCATTGGTTCAGCTTAA-3′.

Fluorescence staining

We performed immunostaining of liver sections and cultured cells using a standard protocol (Kanai et al., 2000). For immunostaining of liver sections, mice were anesthetized and fixed by perfusion with 4% paraformaldehyde in 0.1 M phosphate buffer (pH 7.2). The tissues were cryoprotected with increasing concentrations of sucrose, embedded with O.C.T. embedding medium (Sakura), and frozen in 2-methylbutane cooled with liquid nitrogen. Tissue sections of 15-µm thickness were further fixed with 4% paraformaldehyde in 0.1 M phosphate buffer, and then permeabilized with 0.1% Triton X-100 in PBS. For immunostaining of cultured cells, the cells were fixed with 4% paraformaldehyde in 0.1 M phosphate buffer and then permeabilized with 0.1% Triton X-100 in PBS. After blocking with 1% BSA in PBS, the sections and cells were incubated with primary antibodies in the same buffer, followed by incubation with Alexa Fluor–conjugated secondary antibodies. For double staining using rabbit antibodies (Fig. 3 B; anti-LRP1 and anti-KIF13B antibodies), we used an Alexa Fluor 488–conjugated anti-KIF13B antibody (Invitrogen) as the tertiary antibody in 1% BSA and 10% normal rabbit serum in PBS (Kanai et al., 2004). To investigate the localization of GFP-KIF13B and endocytosed LDL (Fig. 2 E), GFP-KIF13B–transfected cells were rinsed twice with Opti-Mem (Invitrogen), incubated in Opti-MEM containing 10 µg/ml DiI-LDL (Biomedical Technologies) for 7 min at 37°C, immediately rinsed three times with PBS, and fixed with 4% paraformaldehyde in 0.1 M phosphate buffer. Samples were observed under a confocal laser-scanning microscope (LSM-510 Duo; Carl Zeiss) equipped with a C-Apochromat 40×/1.2 W lens (Carl Zeiss). Images were captured by a camera (AxioCamHRc; Carl Zeiss) using its accompanying LSM 510 software (Carl Zeiss) at room temperature. For filipin staining (Fig. 2 F), KO MEFs transfected with GFP-KIF13B were fixed with 4% paraformaldehyde in 0.1 M phosphate buffer. After incubation with 50 µg/ml filipin (Sigma-Aldrich) in PBS at room temperature for 2 h, cells were observed under an microscope (IX70; Olympus) equipped with a UPlanApo 40×/1.00 lens using U-MWU2 (filipin) and U-MNIBA2 (GFP) filter sets (Olympus). Images were captured by a CoolSNAPcf camera (Photometrics) using MetaCam software (Universal Imaging Corp.) at room temperature. Processing of the images and colocalization and vesicle size analyses were performed using ImageJ 1.47 with "Colocalization" and "Particle Analysis (Nucleus Counter)" plugins (National Institutes of Health, Bethesda, MD).

DiI-LDL uptake

WT and KO MEFs (Fig. 2 G), or KO MEFs infected with GFP-KIF13B- or GFP-adenovector and cultured for 6 h after infection along with noninfected KO MEFs (Fig. 2 H), were rinsed twice with Opti-MEM and incubated with Opti-MEM containing 10 µg/ml DiI-LDL for 10, 20, or 40 min (Fig. 2 G), or 20 min (Fig. 2 H) at 37°C. Cells were then rinsed three times with PBS and fixed with 4% paraformaldehyde in 0.1 M phosphate buffer. Cells were stained with DRAQ5 (Cell Signaling Technology) to count the cell number. Intensities of the DiI signal from endocytosed DiI-LDL were measured and the cell numbers in the same field were counted under a confocal laser-scanning microscope (LSM-510 Duo; Carl Zeiss) equipped with a Plan Apochromat 20×/0.8 NA lens (Carl Zeiss). Intensities of DiI signal, subtracted by background level (intensity of non-DiI loaded cells), corrected by cell number, were compared between WT and KO MEFs (Fig. 2 G) or between GFP-KIF13B– or GFP-adenovector infected and noninfected KO MEFs (Fig. 2 H). Processing of the images was performed with ImageJ 1.47.

Blood biochemistry

We used littermate WT and KO adult male mice for the blood biochemical analyses. We anesthetized the mice, opened their chests, and directly obtained blood samples from the left ventricle using 1-ml syringes equipped with a 25-gauge needle. The blood samples were quickly mixed with ice-cold sodium citrate to a final concentration of 10 mM, and centrifuged at 2,000 *g* for 20 min at 4°C. The serum supernatants were used for cholesterol and fVIII analyses. The total serum cholesterol concentrations were measured using a Cholesterol E kit (Wako Chemicals USA) according to the manufacturer's instructions. The cholesterol profiles of the serum lipoproteins were analyzed using a high-sensitivity lipoprotein profiling system with high-performance liquid chromatography (Okazaki et al., 2005) at Skylight Biotech (Akita, Japan). The serum fVIII activities were measured using a clotting time method at SRL, Inc. (Tokyo, Japan).

Immunoprecipitation and protein identification

Immunoprecipitation and protein identification were performed as described previously (Kanai et al., 2004). In brief, WT and KO mouse livers were homogenized in a homogenizing buffer (50 mM Tris-HCl, pH 8.0, 150 mM NaCl, 1% Triton-X, and 0.5% NP-40) supplemented with protease inhibitors (Roche). Homogenates, precleared with Protein G–Sepharose Fast Flow (GE Healthcare), were applied to immunoprecipitation using antibodies and Protein G–Sepharose Fast Flow according to the manufacturer's instructions. To identify the proteins separated on SDS-PAGE gels, bands excised and digested with trypsin (Roche) were subjected to a 4700 Proteomics Analyzer (Applied Biosystems).

Binding assay

FLAG-tagged full-length or truncated utrophin and myc-tagged full-length or truncated KIF13B were cotransfected in HEK293A cells. Cells, cultured for 16 h after transfection, were lysed in the homogenizing buffer, followed by immunoprecipitation using anti-myc and anti-FLAG antibodies. The precipitants, separated on SDS-PAGE gels, were stained with Coomassie brilliant blue.

Online supplemental material

Fig. S1 shows the targeted disruption of the mouse *kif13b* gene. Fig. S2 shows the histological analyses of major organs from WT and KO mice. Fig. S3 shows the immunoblotting analyses of WT and KO MEFs and livers using antibodies against KIF13B, KIF5B, LRP1, LDLr, hDLG1, and utrophin. Fig. S4 shows quantitative analyses of the size of LRP1-containing vesicles. Online supplemental material is available at http://www.jcb.org/cgi/content/full/jcb.201309066/DC1.

The authors thank H. Fukuda, H. Sato, T. Akamatsu, N. Onouchi, and others from the Hirokawa laboratory for technical assistance. The authors also thank J.M. Ervasti for providing the cDNA of utrophin.

This study was supported by a Grant-in-Aid for Specially Promoted Research to N. Hirokawa and a Global COE Program to The University of Tokyo from the Ministry of Education, Culture, Sports, Science and Technology of Japan.

This paper is dedicated to the late professor Hideko Kanai (Kyoto University of Education, Kyoto, Japan).

Submitted: 13 September 2013
Accepted: 20 December 2013

References

Anderson, C.N.G., and S.G.N. Grant. 2006. High throughput protein expression screening in the nervous system—needs and limitations. *J. Physiol.* 575:367–372. http://dx.doi.org/10.1113/jphysiol.2006.113795

Bolis, A., S. Coviello, I. Visigalli, C. Taveggia, A. Bachi, A.H. Chishti, T. Hanada, A. Quattrini, S.C. Previtali, A. Biffi, and A. Bolino. 2009. Dlg1, Sec8, and Mtmr2 regulate membrane homeostasis in Schwann cell myelination. *J. Neurosci.* 29:8858–8870. http://dx.doi.org/10.1523/JNEUROSCI.1423-09.2009

Bovenschen, N., J. Herz, J.M. Grimbergen, P.J. Lenting, L.M. Havekes, K. Mertens, and B.J.M. van Vlijmen. 2003. Elevated plasma factor VIII in a mouse model of low-density lipoprotein receptor-related protein deficiency. *Blood*. 101:3933–3939. http://dx.doi.org/10.1182/blood-2002-07-2081

Czech, M.P. 2000. PIP2 and PIP3: complex roles at the cell surface. *Cell*. 100:603–606. http://dx.doi.org/10.1016/S0092-8674(00)80696-0

Donaldson, J.G. 2003. Multiple roles for Arf6: sorting, structuring, and signaling at the plasma membrane. *J. Biol. Chem.* 278:41573–41576. http://dx.doi.org/10.1074/jbc.R300026200

Durbeej, M., M.D. Henry, M. Ferletta, K.P. Campbell, and P. Ekblom. 1998. Distribution of dystroglycan in normal adult mouse tissues. *J. Histochem. Cytochem.* 46:449–457. http://dx.doi.org/10.1177/002215549804600404

Franchini, M., and M. Montagnana. 2011. Low-density lipoprotein receptor-related protein 1: new functions for an old molecule. *Clin. Chem. Lab. Med.* 49:967–970. http://dx.doi.org/10.1515/CCLM.2011.154

Fujita, A., and Y. Kurachi. 2000. SAP family proteins. *Biochem. Biophys. Res. Commun.* 269:1–6. http://dx.doi.org/10.1006/bbrc.1999.1893

Guo, W.X., M. Nichol, and J.P. Merlie. 1996. Cloning and expression of full length mouse utrophin: the differential association of utrophin and dystrophin with AChR clusters. *FEBS Lett.* 398:259–264. http://dx.doi.org/10.1016/S0014-5793(96)01216-1

Haenggi, T., and J.-M. Fritschy. 2006. Role of dystrophin and utrophin for assembly and function of the dystrophin glycoprotein complex in non-muscle tissue. *Cell. Mol. Life Sci.* 63:1614–1631. http://dx.doi.org/10.1007/s00018-005-5461-0

Hanada, T., L. Lin, E.V. Tibaldi, E.L. Reinherz, and A.H. Chishti. 2000. GAKIN, a novel kinesin-like protein associates with the human homologue of the Drosophila discs large tumor suppressor in T lymphocytes. *J. Biol. Chem.* 275:28774–28784. http://dx.doi.org/10.1074/jbc.M000715200

Hayer, A., M. Stoeber, D. Ritz, S. Engel, H.H. Meyer, and A. Helenius. 2010. Caveolin-1 is ubiquitinated and targeted to intralumenal vesicles in endolysosomes for degradation. *J. Cell Biol.* 191:615–629. http://dx.doi.org/10.1083/jcb.201003086

Herz, J., and D.K. Strickland. 2001. LRP: a multifunctional scavenger and signaling receptor. *J. Clin. Invest.* 108:779–784.

Herz, J., D.E. Clouthier, and R.E. Hammer. 1992. LDL receptor-related protein internalizes and degrades uPA-PAI-1 complexes and is essential for embryo implantation. *Cell*. 71:411–421. http://dx.doi.org/10.1016/0092-8674(92)90511-A

Hirokawa, N. 1998. Kinesin and dynein superfamily proteins and the mechanism of organelle transport. *Science*. 279:519–526. http://dx.doi.org/10.1126/science.279.5350.519

Hirokawa, N., and Y. Noda. 2008. Intracellular transport and kinesin superfamily proteins, KIFs: structure, function, and dynamics. *Physiol. Rev.* 88:1089–1118. http://dx.doi.org/10.1152/physrev.00023.2007

Hirokawa, N., S. Niwa, and Y. Tanaka. 2010. Molecular motors in neurons: transport mechanisms and roles in brain function, development, and disease. *Neuron*. 68:610–638. http://dx.doi.org/10.1016/j.neuron.2010.09.039

Horiguchi, K., T. Hanada, Y. Fukui, and A.H. Chishti. 2006. Transport of PIP3 by GAKIN, a kinesin-3 family protein, regulates neuronal cell polarity. *J. Cell Biol.* 174:425–436. http://dx.doi.org/10.1083/jcb.200604031

Hsueh, Y.-P. 2006. The role of the MAGUK protein CASK in neural development and synaptic function. *Curr. Med. Chem.* 13:1915–1927. http://dx.doi.org/10.2174/092986706777585040

Ilsley, J.L., M. Sudol, and S.J. Winder. 2002. The WW domain: linking cell signalling to the membrane cytoskeleton. *Cell. Signal.* 14:183–189. http://dx.doi.org/10.1016/S0898-6568(01)00236-4

Jeon, H., and S.C. Blacklow. 2005. Structure and physiologic function of the low-density lipoprotein receptor. *Annu. Rev. Biochem.* 74:535–562. http://dx.doi.org/10.1146/annurev.biochem.74.082803.133354

Kanai, Y., Y. Okada, Y. Tanaka, A. Harada, S. Terada, and N. Hirokawa. 2000. KIF5C, a novel neuronal kinesin enriched in motor neurons. *J. Neurosci.* 20:6374–6384.

Kanai, Y., N. Dohmae, and N. Hirokawa. 2004. Kinesin transports RNA: isolation and characterization of an RNA-transporting granule. *Neuron*. 43:513–525. http://dx.doi.org/10.1016/j.neuron.2004.07.022

Kounnas, M.Z., R.D. Moir, G.W. Rebeck, A.I. Bush, W.S. Argraves, R.E. Tanzi, B.T. Hyman, and D.K. Strickland. 1995. LDL receptor-related protein, a multifunctional ApoE receptor, binds secreted beta-amyloid precursor protein and mediates its degradation. *Cell*. 82:331–340. http://dx.doi.org/10.1016/0092-8674(95)90320-8

Lenting, P.J., J.G. Neels, B.M. van den Berg, P.P. Clijsters, D.W. Meijerman, H. Pannekoek, J.A. van Mourik, K. Mertens, and A.J. van Zonneveld. 1999. The light chain of factor VIII comprises a binding site for low density lipoprotein receptor-related protein. *J. Biol. Chem.* 274:23734–23739. http://dx.doi.org/10.1074/jbc.274.34.23734

Lillis, A.P., L.B. Van Duyn, J.E. Murphy-Ullrich, and D.K. Strickland. 2008. LDL receptor-related protein 1: unique tissue-specific functions revealed by selective gene knockout studies. *Physiol. Rev.* 88:887–918. http://dx.doi.org/10.1152/physrev.00033.2007

Liu, Y., M. Jones, C.M. Hingtgen, G. Bu, N. Laribee, R.E. Tanzi, R.D. Moir, A. Nath, and J.J. He. 2000. Uptake of HIV-1 tat protein mediated by low-density lipoprotein receptor-related protein disrupts the neuronal metabolic balance of the receptor ligands. *Nat. Med.* 6:1380–1387. http://dx.doi.org/10.1038/82199

Miki, H., M. Setou, K. Kaneshiro, and N. Hirokawa. 2001. All kinesin superfamily protein, KIF, genes in mouse and human. *Proc. Natl. Acad. Sci. USA*. 98:7004–7011. http://dx.doi.org/10.1073/pnas.111145398

Nakata, T., and N. Hirokawa. 2003. Microtubules provide directional cues for polarized axonal transport through interaction with kinesin motor head. *J. Cell Biol.* 162:1045–1055. http://dx.doi.org/10.1083/jcb.200302175

Okazaki, M., S. Usui, M. Ishigami, N. Sakai, T. Nakamura, Y. Matsuzawa, and S. Yamashita. 2005. Identification of unique lipoprotein subclasses for visceral obesity by component analysis of cholesterol profile in high-performance liquid chromatography. *Arterioscler. Thromb. Vasc. Biol.* 25:578–584. http://dx.doi.org/10.1161/01.ATV.0000155017.60171.88

Pelkmans, L., and A. Helenius. 2002. Endocytosis via caveolae. *Traffic*. 3:311–320. http://dx.doi.org/10.1034/j.1600-0854.2002.30501.x

Ramírez-Sánchez, I., P. Mendoza-Lorenzo, A. Zentella-Dehesa, E. Méndez-Bolaina, E. Lara-Padilla, G. Ceballos-Reyes, P. Canto, C. Palma-Flores, and R.M. Coral-Vázquez. 2012. Caveolae and non-caveolae lipid raft microdomains of human umbilical vein endothelial cells contain utrophin-associated protein complexes. *Biochimie*. 94:1884–1890. http://dx.doi.org/10.1016/j.biochi.2012.05.001

Saenko, E.L., A.V. Yakhyaev, I. Mikhailenko, D.K. Strickland, and A.G. Sarafanov. 1999. Role of the low density lipoprotein-related protein receptor in mediation of factor VIII catabolism. *J. Biol. Chem.* 274:37685–37692. http://dx.doi.org/10.1074/jbc.274.53.37685

Sotgia, F., J.K. Lee, K. Das, M. Bedford, T.C. Petrucci, P. Macioce, M. Sargiacomo, F.D. Bricarelli, C. Minetti, M. Sudol, and M.P. Lisanti. 2000. Caveolin-3 directly interacts with the C-terminal tail of beta -dystroglycan. Identification of a central WW-like domain within caveolin family members. *J. Biol. Chem.* 275:38048–38058. http://dx.doi.org/10.1074/jbc.M005321200

Steinmetz, M.O., and A. Akhmanova. 2008. Capturing protein tails by CAP-Gly domains. *Trends Biochem. Sci.* 33:535–545. http://dx.doi.org/10.1016/j.tibs.2008.08.006

Takahashi, J., Y. Itoh, K. Fujimori, M. Imamura, Y. Wakayama, Y. Miyagoe-Suzuki, and S. Takeda. 2005. The utrophin promoter A drives high expression of the transgenic LacZ gene in liver, testis, colon, submandibular gland, and small intestine. *J. Gene Med.* 7:237–248. http://dx.doi.org/10.1002/jgm.651

Tinsley, J.M., D.J. Blake, A. Roche, U. Fairbrother, J. Riss, B.C. Byth, A.E. Knight, J. Kendrick-Jones, G.K. Suthers, D.R. Love, et al. 1992. Primary structure of dystrophin-related protein. *Nature*. 360:591–593. http://dx.doi.org/10.1038/360591a0

Ueno, H., X. Huang, Y. Tanaka, and N. Hirokawa. 2011. KIF16B/Rab14 molecular motor complex is critical for early embryonic development by transporting FGF receptor. *Dev. Cell*. 20:60–71. http://dx.doi.org/10.1016/j.devcel.2010.11.008

Vale, R.D. 2003. The molecular motor toolbox for intracellular transport. *Cell*. 112:467–480. http://dx.doi.org/10.1016/S0092-8674(03)00111-9

Venkateswarlu, K., T. Hanada, and A.H. Chishti. 2005. Centaurin-alpha1 interacts directly with kinesin motor protein KIF13B. *J. Cell Sci.* 118:2471–2484. http://dx.doi.org/10.1242/jcs.02369

Venkateswarlu, K., K.G. Brandom, and H. Yun. 2007. PI-3-kinase-dependent membrane recruitment of centaurin-alpha2 is essential for its effect on ARF6-mediated actin cytoskeleton reorganisation. *J. Cell Sci.* 120:792–801. http://dx.doi.org/10.1242/jcs.03373

Wang, X., S.-R. Lee, K. Arai, S.-R. Lee, K. Tsuji, G.W. Rebeck, and E.H. Lo. 2003. Lipoprotein receptor-mediated induction of matrix metalloproteinase by tissue plasminogen activator. *Nat. Med.* 9:1313–1317. http://dx.doi.org/10.1038/nm926

Yamada, K.H., T. Hanada, and A.H. Chishti. 2007. The effector domain of human Dlg tumor suppressor acts as a switch that relieves autoinhibition of kinesin-3 motor GAKIN/KIF13B. *Biochemistry*. 46:10039–10045. http://dx.doi.org/10.1021/bi701169w

Zhang, H., P.H. Links, J.K. Ngsee, K. Tran, Z. Cui, K.W.S. Ko, and Z. Yao. 2004. Localization of low density lipoprotein receptor-related protein 1 to caveolae in 3T3-L1 adipocytes in response to insulin treatment. *J. Biol. Chem.* 279:2221–2230. http://dx.doi.org/10.1074/jbc.M310679200